Science Advances
AAAS

advances.sciencemag.org/cgi/content/full/6/22/eaay7148/DC1

Supplementary Materials for

Treatment of severe sepsis with nanoparticulate cell-free DNA scavengers

Jianati Dawulieti, Madi Sun, Yawei Zhao, Dan Shao*, Huize Yan, Yeh-Hsing Lao, Hanze Hu, Lianzhi Cui, Xiaoyan Lv, Feng Liu, Chun-Wei Chi, Yue Zhang, Mingqiang Li, Ming Zhang, Huayu Tian, Xuesi Chen, Kam W. Leong*, Li Chen*

*Corresponding author. Email: chenl@jlu.edu.cn (L.Ch.); stanauagate@outlook.com (D.S.); kam.leong@columbia.edu (K.W.L.)

Published 29 May 2020, *Sci. Adv.* **6**, eaay7148 (2020)
DOI: 10.1126/sciadv.aay7148

This PDF file includes:

MATERIALS AND METHODS

Materials and Reagents

Generation 3.0 polyamidoamine dendrimer (PAMAM-G3), branched polyethylenimine (PEI, Mw= 25000), branched polyethylenimine (PEI, Mw= 7800), calf thymus DNA (ct-DNA), tetraethyl orthosilicate (TEOS), bis[3-(triethoxysilyl)propyl]tetrasulfide (BTESPT), etyltrimethylammonium tosylate (CTAT), triethanolamine (TEAH3), (3-glycidyloxypropyl)trimethoxysilane (3-GPS), 3-aminopropyltriethoxysilane (APTES), fluorescein isothiocyanate (FITC), D-galactosamine (D-GalN), and reduced glutathione (GSH) were purchased from Sigma-Aldrich (St. Louis, MO, U.S.A.). LysoTracker Red DND-99 and 4',6-diamidino-2-phenylindole (DAPI) were purchased from Invitrogen Co. (Carlsbad, CA, U.S.A.). Cyanine 7 succinimidyl ester (Cy7-NHS) and fluorescein isothiocyanate succinimidyl ester (FITC-NHS) were purchased from Lumiprobe Corporation (Hallandale Beach, FL, U.S.A.). Dulbecco's modified Eagle's medium (DMEM), fetal bovine serum (FPS), and 0.25% trypsin-EDTA were purchased from Gibco Co., Ltd. (Carlsbad, CA, U.S.A.). Antibiotic/antimycotic solution was purchased form Life Technologies, Inc. (Grand Island, NY, U.S.A.). Quant-iT™ PicoGreen™ dsDNA Assay Kit, Promega™ CellTiter 96™ AQueous One Solution Cell Proliferation Assay (MTS) Kit, DNeasy Blood & Tissue Kit, and Sodium Pyruvate 100 mM Solution were purchased from Fisher Scientific Inc. (Pittsburgh, PA, U.S.A.). CpG 1826 and Cy5.5 labeled-CpG 1826 were purchased from Integrated DNA Technologies (IDT, Coralville, IA, U.S.A.). All the other reagents were commercially available and used as received.

BD Cytofix/Cytoperm™ Fixation/Permeabilization Solution Kit was purchased from BD Biosciences. TruStain FcX™ (anti-mouse CD16/32) Antibody (clone 93) were purchased from Biolegend. F4/80 monoclonal antibody (cat. #11-4801-82), rat IgG2a kappa isotype control (cat. #11-4321-81), CD11c monoclonal antibody, (cat. #12-0114-82), armenian hamster IgG isotype control (cat. #12-4888-81) and CD289 (TLR9) monoclonal antibody (cat. #11-9093-82) were purchased from eBioscience™. GAPDH mouse monoclonal antibody (cat. #60004-1-Ig) was purchased from Proteintech. Anti-NF-kB p65 (phospho S536) antibody (cat. #ab28856), anti-NF-kB p65 antibody (cat. #ab16502), anti-MyD88 antibody (cat. #ab135693) and anti-TLR9 antibody (cat. #ab134368) were purchased from Abcam. BCA protein assay kit was purchased from Thermo Fisher Scientific. TNF-α (cat. # KE10002), IL-6 (cat. # KE10007) and MCP-1 (cat.

KE10006) were purchased from Proteintech. Trizol reagent was purchased from Invitrogen. SYBR green qPCR assay was purchased from Roche. cDNA synthesis kit was purchased from Transgen Biotech, China. All the primers were synthesized by Sangon Biotech, China.

GAPDH Forward sense:TGTGTCCGTCGTGGATCTGA;

GAPDH Reverse sense:CCTGCTTCACCACCTTCTTGAT;

TNF-α Forward sense:CACGTCGTAGCAAACCACC;

TNF-α Reverse sense:TGAGATCCATGCCGTTGGC;

iNOS Forward sense:GAATCTTGGAGCGAGTTGTGG;

iNOS Reverse sense:AGGAAGTAGGTGAGGGCTTGG;

Arg-1 Forward sense:CCGCAGCATTAAGGAAAGC;

Arg-1 Reverse sense:CCCGTGGTCTCTCACATTG.

CpG 1826: (5'-TCCATGACGTTCCTGACGTT-3')

CpG-induced SIRS models

The CpG-induced SIRS model in male BALB/c mice was constructed as previously described (*26*). Briefly, 1 h after sensitization with D-GalN (800 mg/kg, i.p.), mice (n=6-8) were administered CpG 1826 (4 mg/kg, i.p.). PAMAM-G3 (20 mg/kg, i.p.) was intraperitoneally injected 30 min after CpG 1826 administration. Mice were monitored for survival rate as described above, and serum was collected 8 hours after CpG injection for analysis of TNF-α and IL-6 via ELISA. $TLR9^+$ peritoneal cells were analyzed using CD289 (TLR9) monoclonal antibody..

Synthesis of MSN-NH_2

Amino groups were introduced into MSN by suspending 400 mg of MSN in 160 mL of ethanol under sonication. The solution was then stirred at 80 °C for 3 h and cooled to room temperature, followed by the addition of 400 μL of 3-aminopropyltriethoxysilane (APTES). The mixture was stirred at room temperature for 1 h and then refluxed at 80 °C for another 12 h. The MSNs-NH_2 were collected, washed, and dried for further use.

Synthesis of dye-labeled MSN-PEI or PEI

Cy7-NHS and FITC-NHS were used to prepare dye-labeled MSN-PEI or PEI. Briefly, 1 mg of Cy7-NHS or FITC-NHS was added to 10 mg of MSN-PEI or PEI (total concentration 2 mg/mL in 10 mM sodium bicarbonate, pH=8), and the mixture was shaken overnight at 4 °C, followed by removal of the unreacted dye molecules via centrifugation without or with a centrifugal filter unit for MSN-PEI or PEI, respectively.

Characterization

The morphology of MSN was characterized using a JEM-2100F transmission electron microscope (TEM, JEOL, Ltd., Japan). Energy-dispersive X-ray spectroscopy (EDX) was also performed using a JEM-2100F EDX system. The hydrodynamic diameter and zeta potential of the NABMs or NABPs were characterized three times using a Nano-ZS 90 Nanosizer (Malvern Instruments Ltd., Worcestershire, UK). The specific surface area and pore size distribution were evaluated and calculated through Brunauer-Emmett-Teller (BET) and Barrett-Joyner-Halenda (BJH) methods. The PEI content was determined by thermogravimetric analysis (TGA). Degradation of MSN (100 μg/mL) was evaluated in 5 mM of GSH solution at 37 °C under constant rotation. At predetermined times points (0, 1 and 3 days), samples were collected for TEM.

DNA release and *In vitro* TLR9 activation assay of DNA/scavenger complex

ctDNA were mixed with excess scavenger (PAMAM-G3, PEI 25K, PEI 800, MSN-PEI 25K, and MSN-PEI 800) solution. The mixture was shaken for 30 min in the dark to form DNA/scavenger complex. Then, the free DNA on the supernatant was removed by centrifuge (10000 g), and detected via PicoGreen™ dsDNA Assay Kit. The complex of each group was put into 10 mL of Tris solution under different pH values (pH = 7.4, 5.5). Then, the release process was performed at 37 °C under constant rotation. At the designated intervals, the amount of released DNA was monitored.

1 μg/mL CpG 1826/Scavenger complex was incubated with HEK-Blue™ TLR9 reporter cells at a density of 5×10^4/well in a 96-well plate for 24 h, the supernatants were collected and incubated with QUANTI-Blue™ (Invivogen, SanDiego, CA) according to the manufacturer's instructions. The corresponding embryonic alkaline phosphatase (SEAP) activity in each well was quantified by measuring the OD at 620 nm with a multiwall plate reader.

Biochemical parameters, proinflammatory cytokines, and histology

Alanine transaminase (ALT), aspartate transaminase (AST), total bilirubin (TBIL), blood urea nitrogen (BUN), creatinine (CRE), and phosphocreatine kinase (CK) were measured on a Hitachi automatic biochemical analyzer 7180 (Japan) with reagents and settings recommended by the manufacturer. The TNF-α, IL-6 and MCP-1 levels were measured using an ELISA kit. Tissue sections of each organ were stained with hematoxylin and eosin (H&E) and observed. Histopathological changes in the lung, kidney, liver, and heart were blindly reviewed by two independent pathologists. The injury scores were determined according to a previously established method (*52*, *53*), and the detailed criteria are shown in the following.

Liver injury score parameters

Index	0	1	2	3	Maximum
Necrosis	None	Focal piecemeal	Continuous <50%	Continuous >50%	3
Bleeding	None	<30%	30-50%	>50%	3
Infiltration	None	2- to 3-fold	3-to 10-fold	>10-fold	3

Kidney injury score parameters

Renal tubule injury and glomerular shrinkage	Index
None	0
<10%	1
11–25%	2
26–45%	3
46–75%	4
>76%	5

Lung injury score parameters

Changes in lung tissue structure	Index
None	1
Focal interstitial congestion and inflammatory cell	2

infiltration <50%	
Diffuse interstitial congestion and inflammatory cell infiltration >50%	3
Focal consolidation and inflammatory cell infiltration <50%	4
Diffuse consolidation and inflammatory cell infiltration >50%	5

Heart injury score parameters

Changes in cardiac tissue structure	Index
None	0
Focal perivascular and/or interstitial infiltrate without myocyte damage	1
Diffuse infiltrate without myocyte damage	2
One focus of infiltrate with associated myocyte damage	3
Multifocal infiltrate with myocyte damage	4
Diffuse infiltrate with myocyte damage	5
Diffuse, polymorphous infiltrate with extensive myocyte damage±edema, ±hemorrhage+vasculitis	6

In vitro cytotoxicity assay

HUVECs were maintained in DMEM supplemented with 10% FBS, 1 mM sodium pyruvate, and 1% penicillin-streptomycin cocktail. RAW264.7 cells and HUVECs were seeded into 96-well culture plates at a density of 2×10^4/well and cultured until the cells were fully attached. Then, the cells were treated with different concentrations of NABMs or NABPs for 24 h. Next, 20 μL MTT (5 mg/mL^{-1}) was added to each well and incubated with cells for 4 h. Finally, the culture medium was removed, and 150 μL of DMSO was added to dissolve the formazan crystals. The absorption density was measured at a wavelength of 490 nm. Untreated cells were used as a control.

Repeated-dose toxicity of MSN-PEI and PEI

For the subsequent repeated-dose toxicity study, mice were i.p. injected with different NABNs or NABPs doses at 0, 13 and 24 h (n = 10). The mouse mortality was recorded for 14 days. Then, the mice treated with a 20 mg/kg dose were sacrificed at 24 h and 7 days after the last injection. The blood samples were collected at 24 h, and ALT, AST, BUN, CRE, TBIL, and CK levels were measured with Hitachi automatic biochemical analyzer 7180 (Japan). The number of each type of blood cell (RBCs, WBCs and PLTs) was quantified with Sysmex XN-2000 system (Japan). The serum TNF-α, IL-6 and MCP-1 levels were measured with the same ELISA kits (Proteintech, Rosemont, USA) following the manufacturer's instructions. The heart, liver, spleen, kidney and lung tissues were collected at 24 h and on the 7^{th} day after the last injection and fixed with 4% paraformaldehyde. The tissue sections were stained with hematoxylin and eosin and observed.

Flow cytometric analysis

To identify the percentage of macrophages in peritoneal fluid, the peritoneal fluid was collected as described above. The cells were incubated with FcBlock (TruStain FcX™ anti-mouse CD16/32) for 10 min on ice to avoid nonspecific binding. Staining was then performed using an F4/80 monoclonal antibody or Rat IgG2a kappa isotype control for 30 min at 4 °C. After washing, cells were analyzed by FACS (BD Accuri® C6).

With the purpose of determining the percentage of M1 polarized macrophages in peritoneal fluid, the prepared peritoneal cells were similarly incubated with FcBlock (anti-mouse CD16/CD32 antibody) for 10 min first on ice to avoid nonspecific binding, and subsequently the samples were stained with F4/80 monoclonal antibody and CD11c monoclonal antibody for 30 min at 4 °C. A rat IgG2a kappa isotype control and Armenian hamster IgG isotype control were also used; the stained cell samples were analyzed by FACS (BD Accuri® C6) as well.

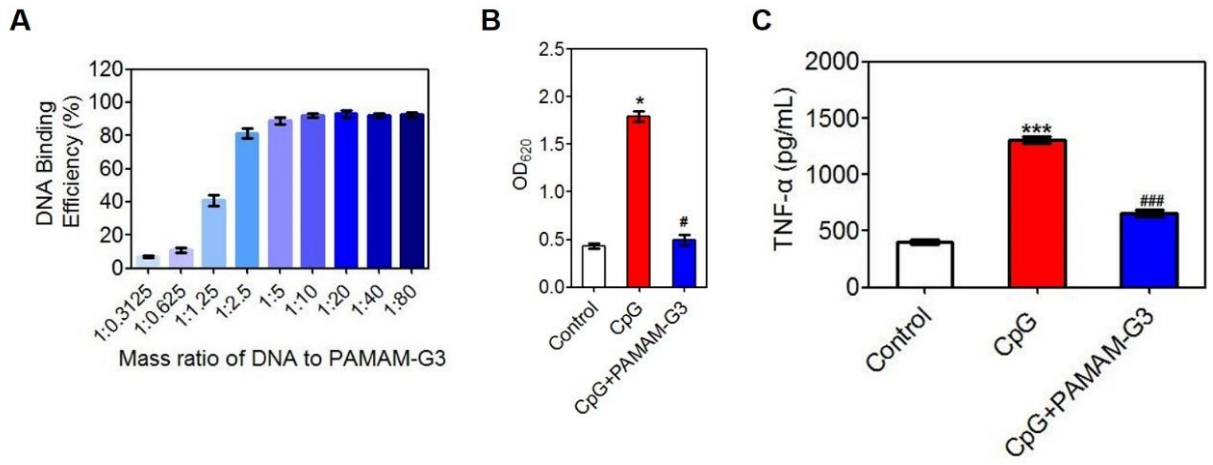

Fig. S1. PAMAM-G3 limits cfDNA-driven proinflammatory response *in vitro*. (**A**) Calf thymus DNA binding efficiency of PAMAM-G3 with different mass ratios at 37 °C. The data are expressed as the means ± SEM (n=3 independent experiments in triplicate). (**B**) Activation of HEK-TLR9 reporter cells by CpG in the absence or presence of PAMAM-G3 (10 μg/mL) for 24 hours. The corresponding embryonic alkaline phosphatase (SEAP) activity in supernatants from each group was determined with a QUANTI-Blue™ assay at OD_{620}. (**C**) RAW 264.7 macrophages were stimulated with CpG in the absence or presence of PAMAM-G3 (10 μg/mL) for 24 hours. Supernatants were assayed for TNF-α via enzyme-linked immunosorbent assay (ELISA). In **B** and **C**, differences were assessed via one-way analysis of variance (ANOVA) with Tukey's multiple comparison tests ($^{*}P<0.05$, $^{***}P<0.001$, compared with control; $^{\#}P<0.05$, $^{\#\#\#}P<0.001$, compared with CpG). The data are expressed as the means ± SEM.

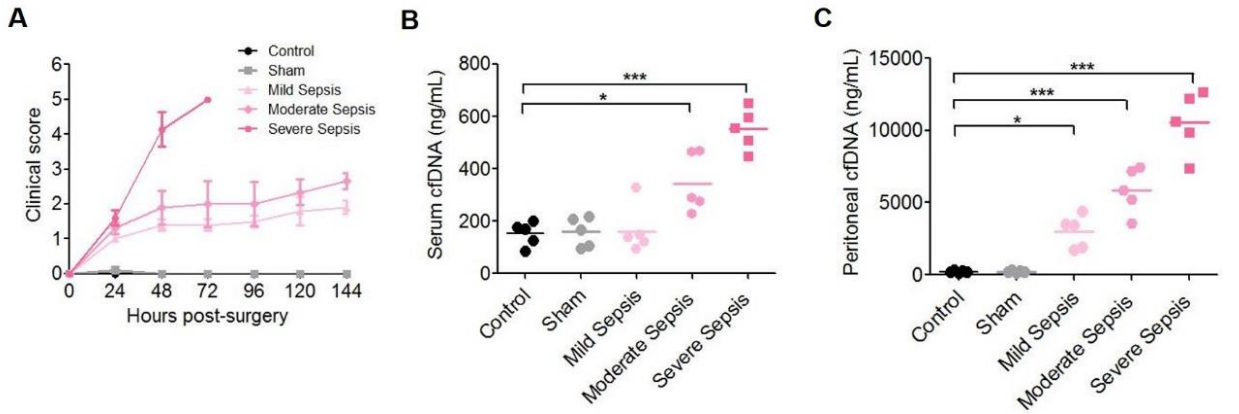

Fig. S2. The highest clinical score and serum and peritoneal cfDNA levels were observed in septic mice with a severe grade. (**A**) After being subjected to CLP of different grades, mice were monitored for 144 hours for clinical scoring. The clinical scoring of sepsis was defined according to a range from 0 (no symptoms) to 5 (loss of self-righting reflex). Mice were scored every 12 hours using the following criteria: score 0, no symptoms; score 1, piloerection and huddling; score 2, piloerection, diarrhea, and huddling; score 3, lack of interest in surroundings and severe diarrhea; score 4, decreased movement and listless appearance; and score 5, loss of self-righting reflex. The data are expressed as the means ± SEM. At 24 h after CLP, (**B**) serum and (**C**) peritoneal cfDNA levels were measured. Differences were assessed via one-way analysis of variance (ANOVA) with Tukey's multiple comparison tests (n=5 mice per group; $^{*}P<0.05$, $^{**}P<0.01$, $^{***}P<0.001$). The data are expressed as the means ± SEM.

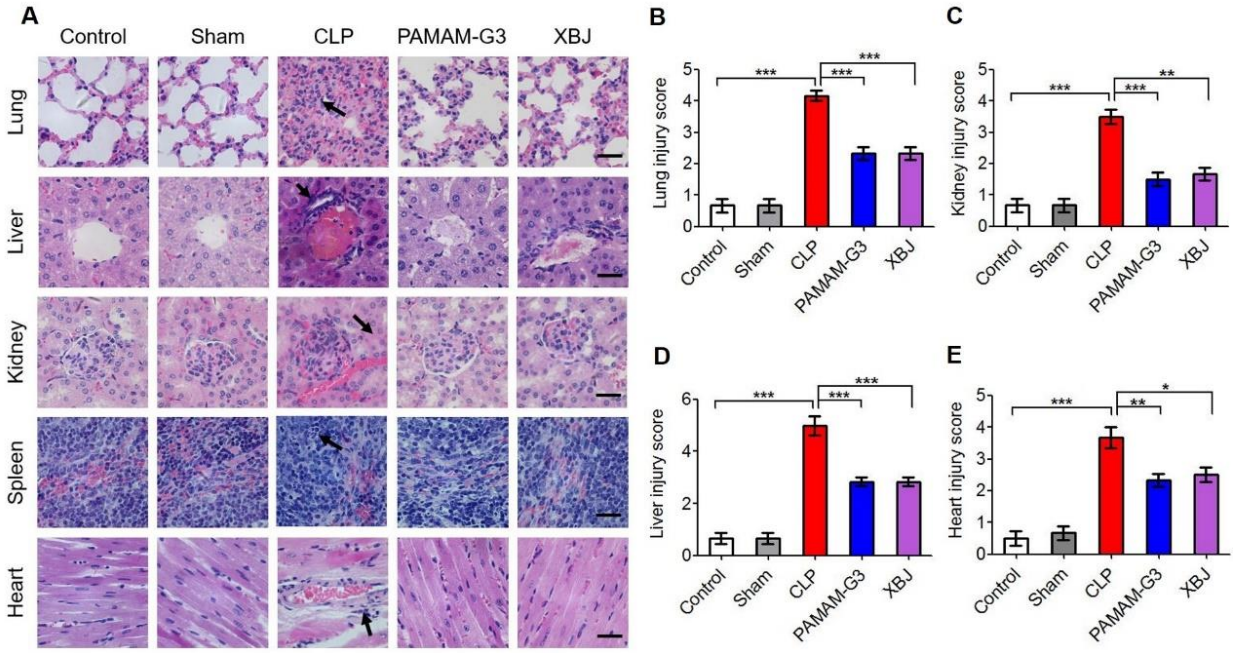

Fig. S3. PAMAM-G3 attenuates multiple organ injury in CLP-induced severe sepsis. High-grade CLP was performed on BALB/c mice, followed by intraperitoneal injection of 20 mg/kg PAMAM-G3 or XBJ 12 hours before and 1 hour and 12 hours after surgery. **(A)** At 24 h after CLP, the lung, kidney, heart, liver and spleen tissues were collected, stained with hematoxylin and eosin (H&E) (scale bars, 20 μm) and analyzed. Multiple organ injury representations, including interalveolar septum thickened in lung, inflammatory cell infiltration in liver and heart, and nuclear debris from dying cells in spleen, are marked with an arrow. The corresponding (**B**) lung, (**C**) kidney, (**D**) liver and (**E**) heart injury scores were determined and calculated according to the established criteria. Differences were assessed via one-way analysis of variance (ANOVA) with Tukey's multiple comparison tests (n=6 mice per group; $^{*}P<0.05$, $^{**}P<0.01$, $^{***}P<0.001$). The data are expressed as the means ± SEM.

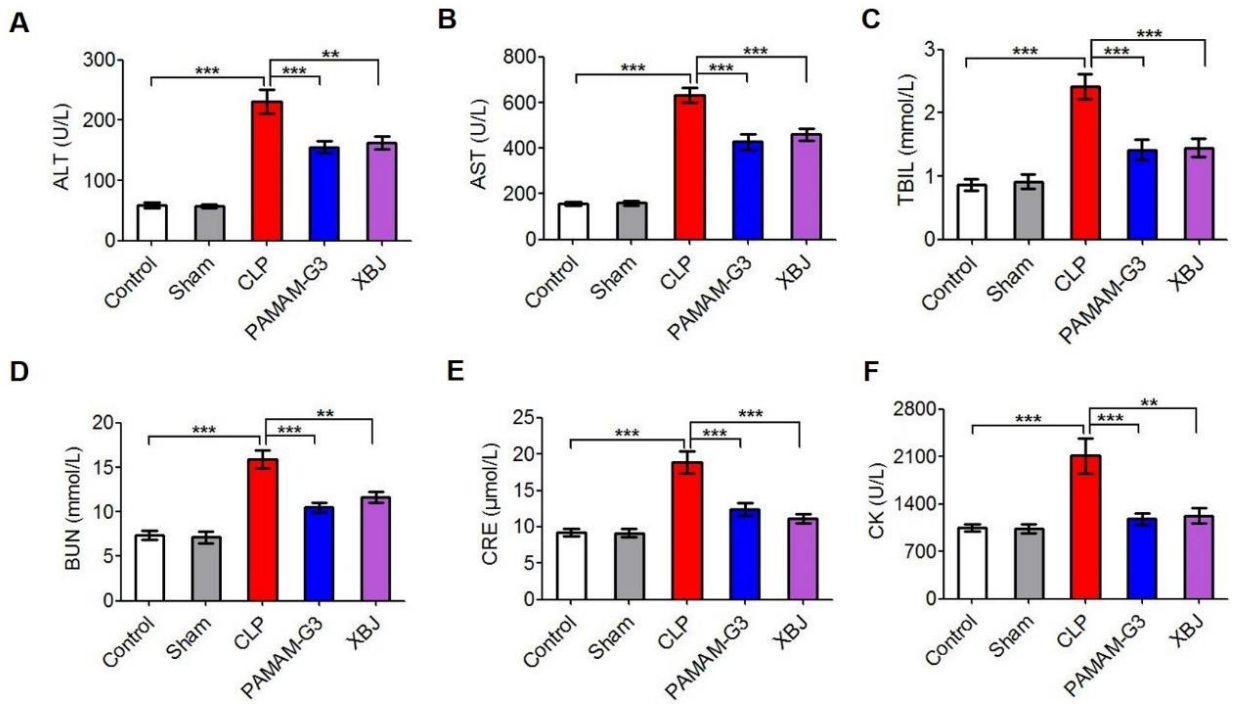

Fig. S4. PAMAM-G3 attenuates biochemistry parameters in CLP-induced severe sepsis. High-grade CLP was performed on BALB/c mice, followed by intraperitoneal injection of 20 mg/kg PAMAM-G3 or XBJ 12 hours before and 1 hour and 12 hours after surgery. The blood serum biochemistry parameters (**A**) ALT, (**B**) AST, (**C**) TBIL, (**D**) BUN, (**E**) CRE, and (**F**) CK were measured. Differences were assessed via one-way analysis of variance (ANOVA) with Tukey's multiple comparison tests (n=6 mice per group; $^{*}P<0.05$, $^{**}P<0.01$, $^{***}P<0.001$). The data are expressed as the means ± SEM.

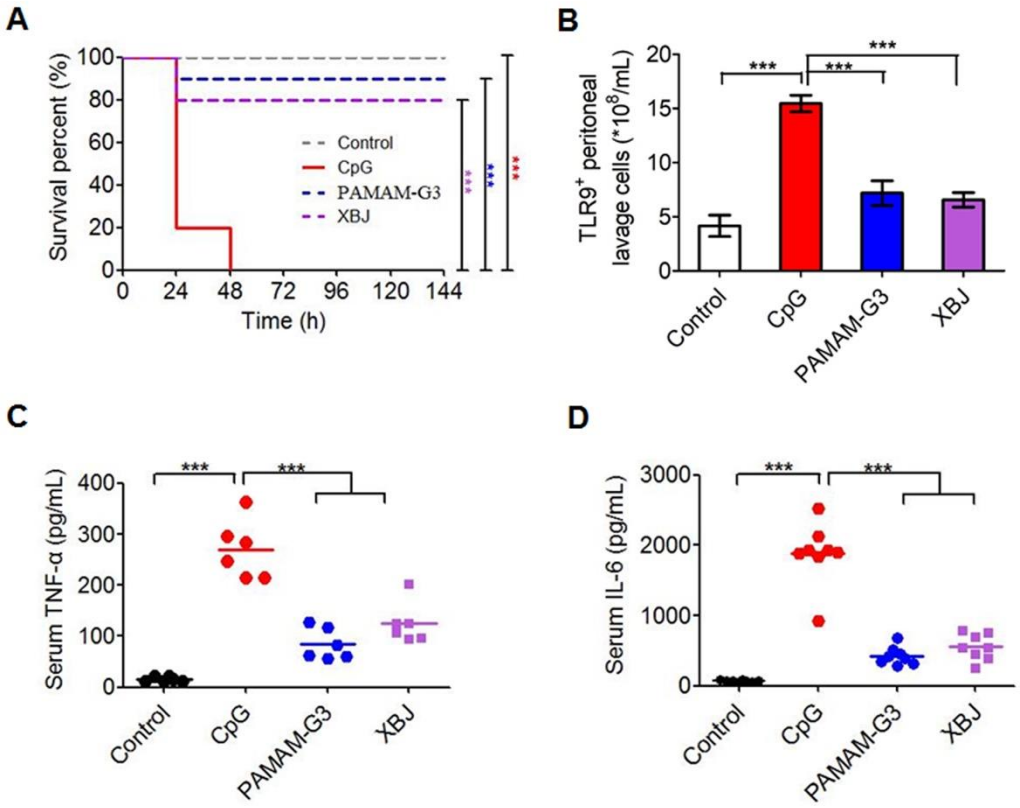

Fig. S5. PAMAM-G3 protects mice against CpG-induced SIRS. (**A**) The CpG-induced SIRS model was constructed in BALB/c mice, followed by intraperitoneal injection of 20 mg/kg PAMAM-G3 or XBJ 30 min after CpG challenge. Survival was monitored for 144 hours (n=10 mice per group; $^{*}P<0.05$, $^{***}P<0.001$, Kaplan-Meier survival analysis). The number of (**B**) $TLR9^{+}$ cells in PLF and the levels of the proinflammatory cytokines (**C**) TNF-α and (**D**) IL-6 in serum were measured 8 h after CpG injection. Differences were assessed via one-way analysis of variance (ANOVA) with Tukey's multiple comparison tests (n=6-8 mice per group; $^{*}P<0.05$, $^{**}P<0.01$, $^{***}P<0.001$). The data are expressed as the means ± SEM.

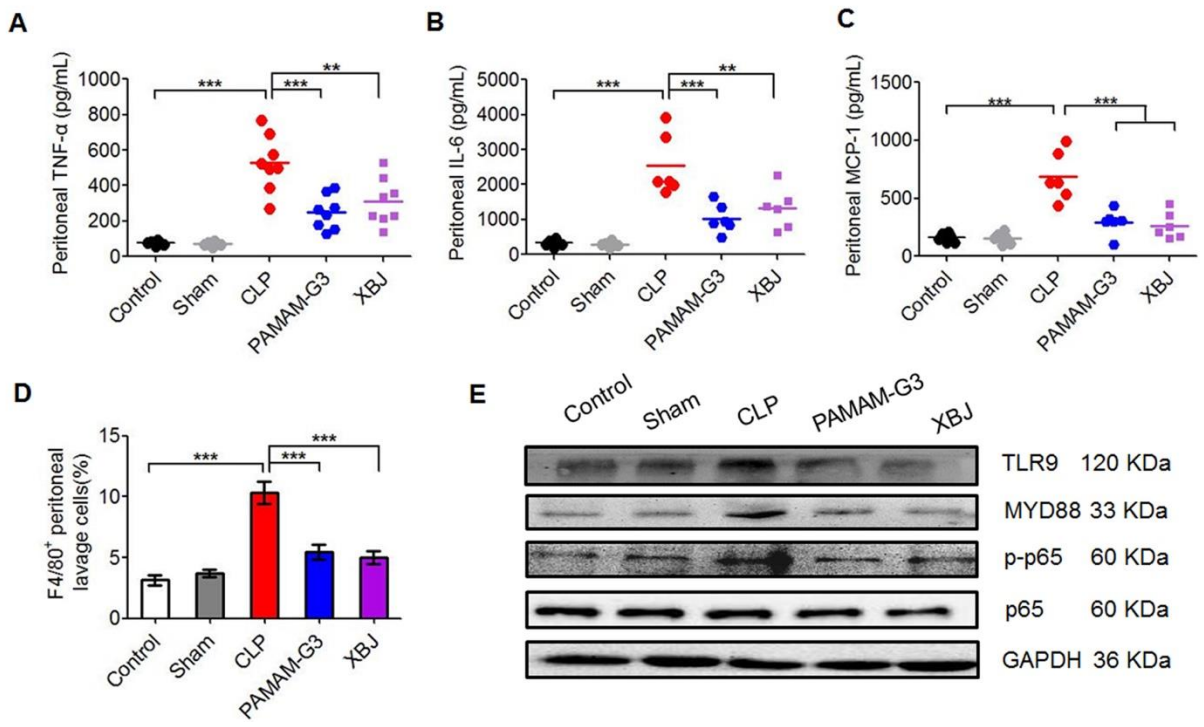

Fig. S6. PAMAM-G3 reverses M1 polarization of peritoneal macrophages through the TLR9-MyD88-NF-κB signaling pathway during severe sepsis. High-grade CLP was performed on BALB/c mice, followed by intraperitoneal injection of 20 mg/kg PAMAM-G3 or XBJ 12 hours before and 1 hour and 12 hours after surgery. Levels of the proinflammatory cytokines (**A**) TNF-α, (**B**) IL-6, and (**C**) MCP-1 were measured in peritoneal lavage fluid (PLF) 24 h post CLP. Immune cell recruitment to the peritoneal cavity was assessed by flow cytometry 8 h post CLP. Percentage of (**D**) peritoneal macrophages ($F4/80^+$) in PLF. Differences were assessed via one-way analysis of variance (ANOVA) with Tukey's multiple comparison tests (n=6 mice per group; $^*P<0.05$, $^{**}P<0.01$, $^{***}P<0.001$). The data are expressed as the means ± SEM. (**E**) Peritoneal macrophages were collected 8 h post CLP and lysed in RIPA buffer. The TLR9, MyD88, p-p65, p65 and GAPDH protein expression levels were measured via western blotting.

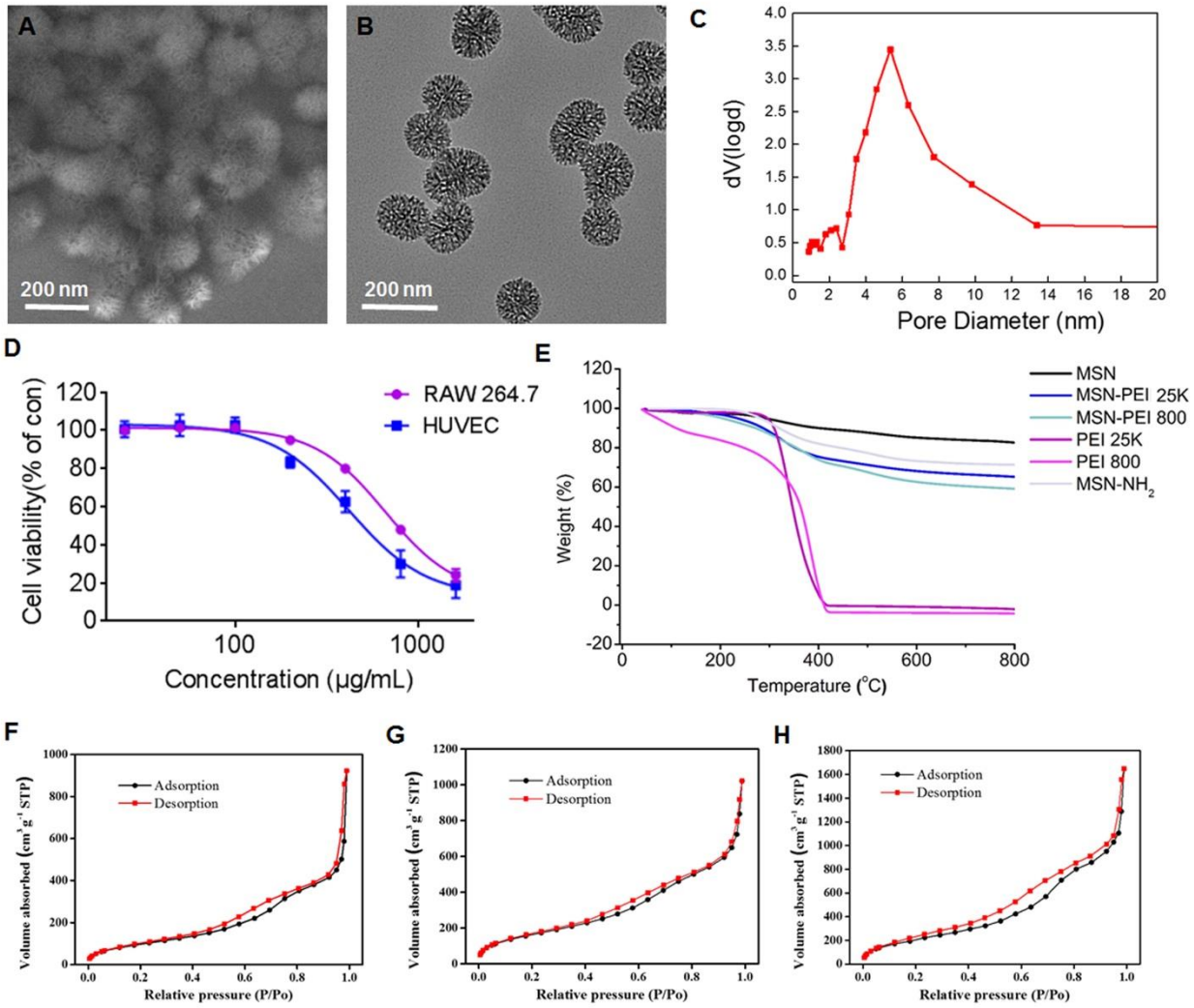

Fig. S7. Characterization and cytotoxicity of MSNs. (**A**) SEM images, (**B**) TEM images, and (C) pore size distributions of MSNs. (**D**) Cell viability of RAW264.7 and HUVEC cells treated with MSNs at various concentrations for 24 h. The data are expressed as the means ± SEM (n=6 independent experiments in triplicate). (**E**) TGA curves of MSN, MSN-PEI 25K, MSN-PEI 800, PEI 25K, PEI 800 and MSN-NH_2. (**F**-**H**) Nitrogen adsorption desorption isotherms of (**F**) MSN-PEI 25K, (**G**) MSN-PEI 800, and (**H**) MSN-NH_2.

Table S1. Characterization of MSN-PEI 25K, MSN-PEI 800, and MSN-NH_2. The Size, Zeta potential, surface area, total pore volume, mass content, and charge density of MSN-PEI 25K, MSN-PEI 800, and MSN-NH_2.

	MSN-PEI 25K	MSN-PEI 800	MSN-NH_2
Size (nm)	156.7 ± 6.6	140.3 ± 5.3	135.1 ± 5.7
Zeta potential (mV)	52.8 ± 1.3	51.9 ± 2.1	35.2 ± 1.5
Surface area (m^2/g)	370.3	618.1	797.1
Total pore volume (cm^3/g)	1.56	1.77	2.85
Mass content (%)	17.30	23.50	11.50
Charge density (μM N/m^2)	10.85	8.55	0.64

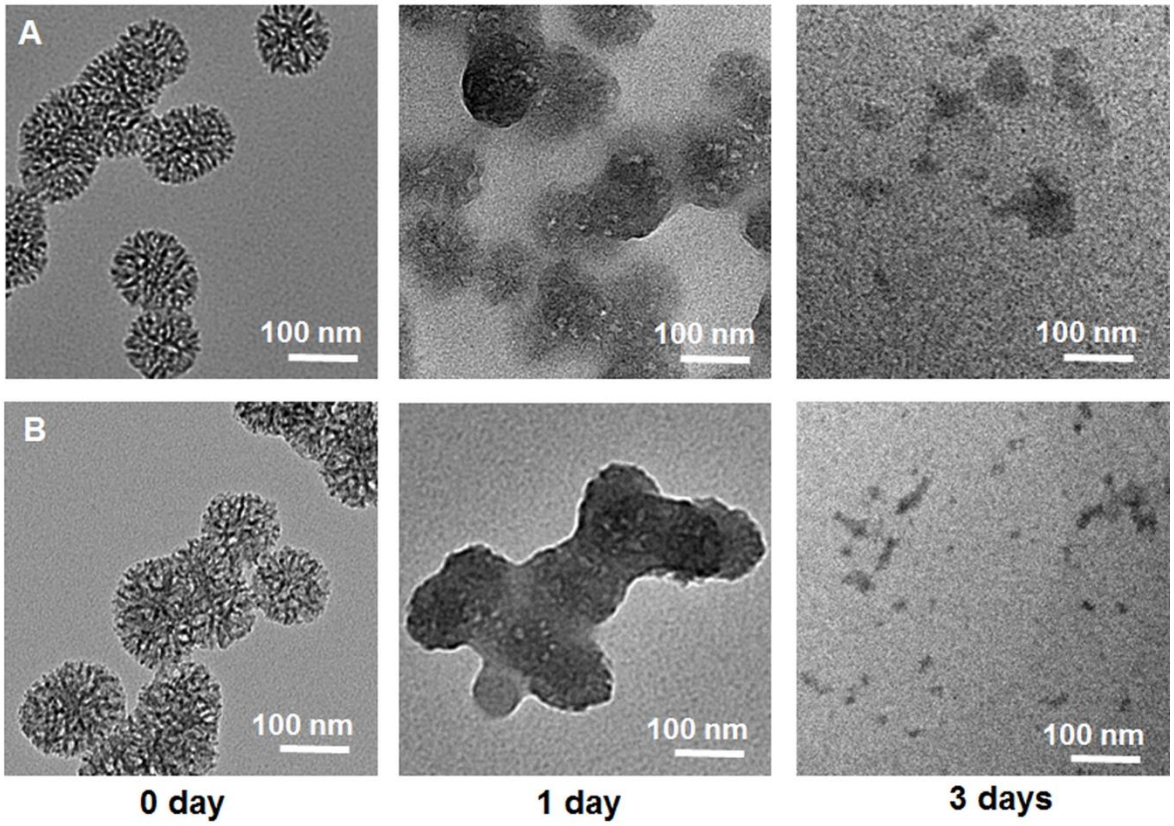

Fig. S8. Degradation of MSNs-PEI. TEM images of (A) MSN-PEI 25K, and (B) MSN-PEI 800 after incubation in buffer containing 5×10^{-3} M GSH for 0, 1 day, and 3 days.

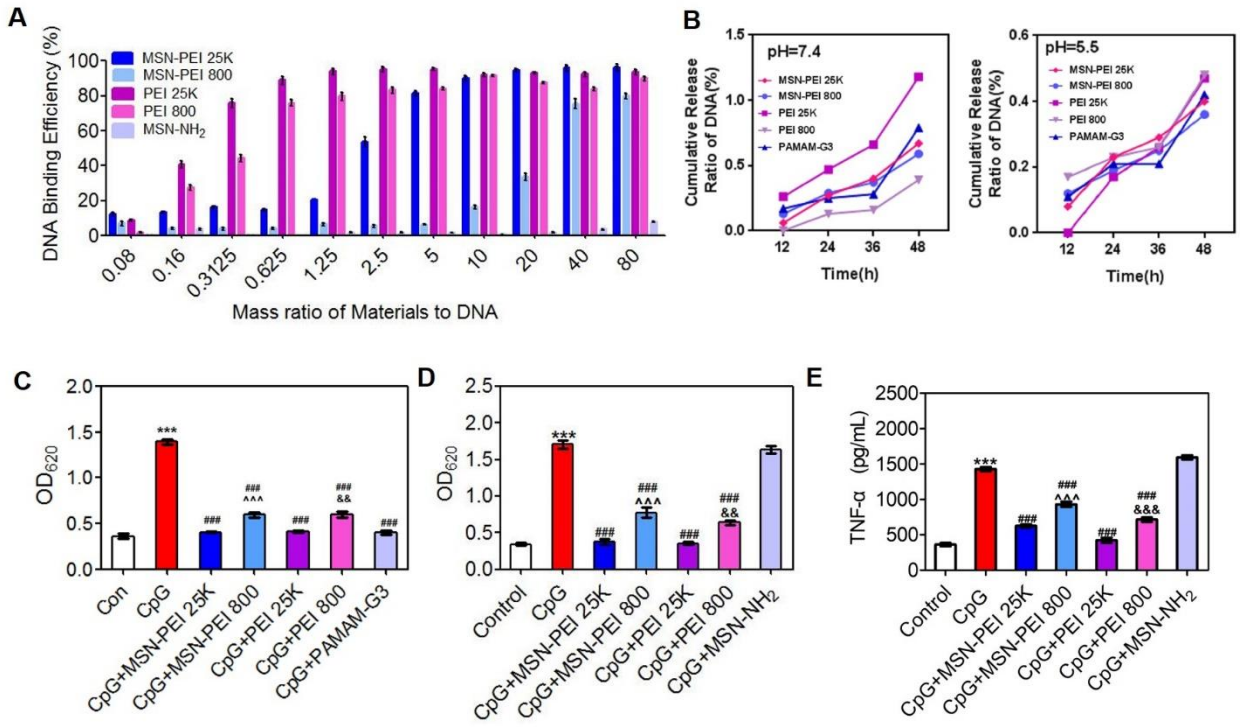

Fig. S9. PEI-functionalized biodegradable MSNs block the pro-inflammatory response *in vitro*. (**A**) Calf thymus DNA binding efficiency of NABNs or NABPs with different mass ratios at 37 °C. The data are expressed as the means ± SEM (n=3 independent experiments in triplicate). (**B**) Release profiles of ctDNA from NABN-DNA or NABP-DNA complex in Tris solution under different pH values for 48 hours. (**C**) Activation of HEK-TLR9 reporter cells by CpG/NABNs or NABPs complex (10 μg/mL) for 24 hours. The corresponding SEAP activity in supernatants from each group was determined with a QUANTI-Blue™ assay at OD_{620}. (**D**) Activation of HEK-TLR9 reporter cells by CpG in the absence or presence of NABNs or NABPs (10 μg/mL) for 24 hours. The corresponding SEAP activity in supernatants from each group was determined with a QUANTI-Blue™ assay at OD_{620}. (**E**) RAW 264.7 macrophages were stimulated with CpG in the absence or presence of NABNs or NABPs (10 μg/mL) for 24 hours. Supernatants were assayed for TNF-α using ELISA. In **C-E**, differences were assessed via one-way analysis of variance (ANOVA) with Tukey's multiple comparison tests ($^{***}P<0.001$, compared with control; $^{###}P<0.001$, compared with CpG; $^{\wedge\wedge\wedge}P<0.001$, compared with CpG+MSN-PEI 25K; $^{\&\&}P<0.01$, $^{\&\&\&}P<0.001$, compared with CpG+PEI 25K). The data are expressed as the means ± SEM (n=3 independent experiments in triplicate).

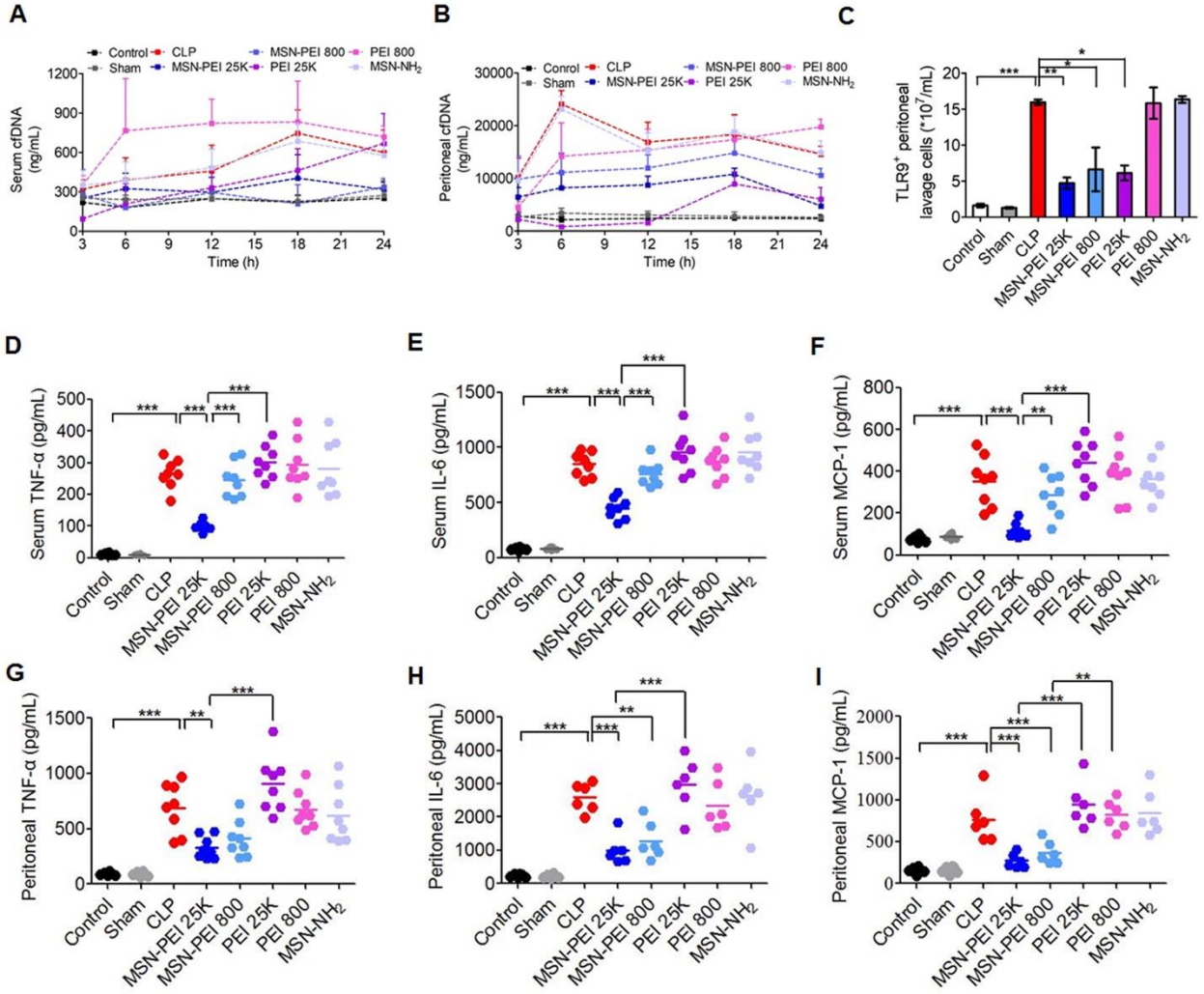

Fig. S10. MSN-PEI 25K protects mice against CLP-induced severe sepsis. High-grade CLP was performed on BALB/c mice, followed by intraperitoneal injection of 20 mg/kg MSN-PEI 25K, MSN-PEI 800, PEI 25K, PEI 800 or MSN-NH_2 12 hours before and 1 hour and 12 hours after surgery. (**A**) serum and (**B**) peritoneal cfDNA levels were measured at 3, 6, 12, 18, and 24-h post CLP. (**C**) The number of $TLR9^+$ cells in PLF was determined by flow cytometry 8 h post CLP. 24 h after CLP, levels of the proinflammatory cytokines (**D**) TNF-α, (**E**) IL-6, and (**F**) MCP-1 in serum, as well as (**G**) TNF-α, (**H**) IL-6, and (**I**) MCP-1 in PLF were measured. Differences were assessed via one-way analysis of variance (ANOVA) with Tukey's multiple comparison tests (n=6-8 mice per group; $^{*}P<0.05$, $^{**}P<0.01$, $^{***}P<0.001$). The data are expressed as the means ± SEM.

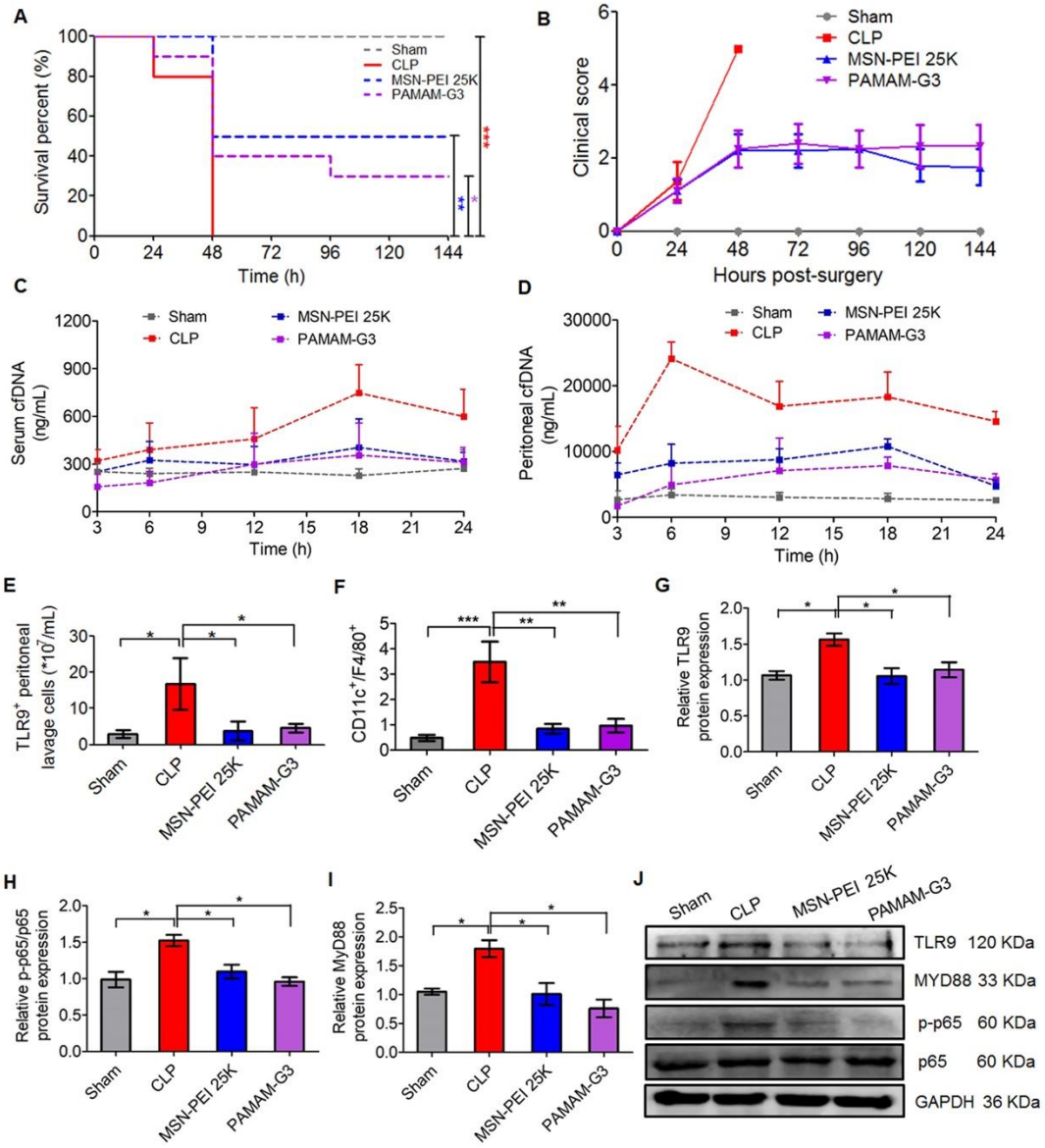

Fig. S11. Comparison of protective effect of PAMAM-G3 and MSN-PEI 25K on CLP-induced severe sepsis. High-grade CLP was performed on BALB/c mice, followed by intraperitoneal injection of 20 mg/kg PAMAM-G3 or MSN-PEI 25K 12 hours before and 1 and 12 hours after surgery. (**A**) Survival was monitored for 144 hours (n=10 mice per group; **P<0.01, ***P<0.001, Kaplan-Meier survival analysis). (**B**) Mice were monitored for 144 hours after CLP for clinical scoring. The data are expressed as the means ± SEM. (**C**) serum and (**D**) peritoneal cfDNA levels were measured at 3, 6, 12, 18, and 24-h post CLP. 8 h after CLP, (**E**) The number of TLR9$^+$ cells and (**F**) the percentage of M1 polarized macrophages (CD11c$^+$F4/80$^+$) were analysed in PLF. In parallel, peritoneal macrophages were collected 8 h post CLP and lysed in RIPA buffer. The (**G**) TLR9, (**H**) MyD88 and (**I**) p-p65 protein expression levels were measured via western blotting (J). The data are expressed as fold change relative to the Sham group and normalized to GAPDH or p65 protein expression. Differences were assessed via one-way analysis of variance (ANOVA) with Tukey's multiple comparison tests (n=5-6 mice per group; *P<0.05, **P<0.01, ***P<0.001). The data are expressed as the means ± SEM.

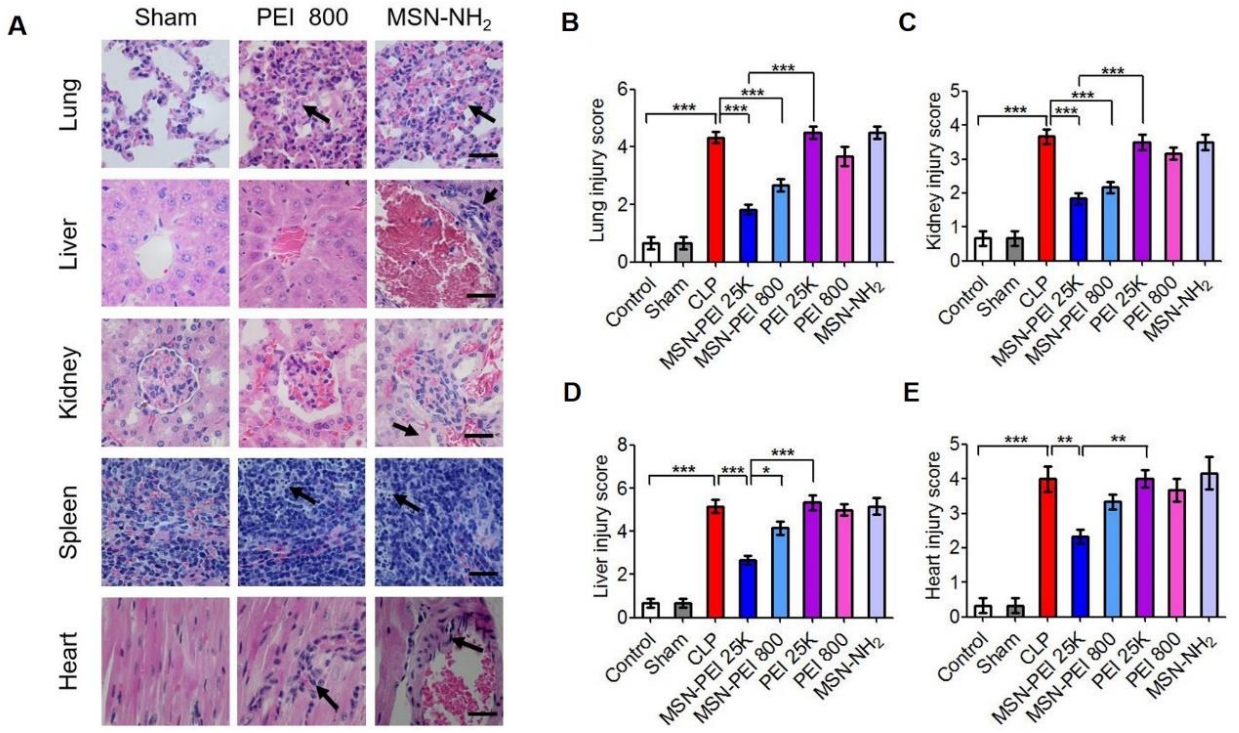

Fig. S12. MSN-PEI 25K attenuates multiple organ injury in CLP-induced severe sepsis. High-grade CLP was performed on BALB/c mice, followed by treatment as described in **Fig. 4**. (**A**) 24 h after CLP, the lung, kidney, heart, liver and spleen tissues were collected, stained with hematoxylin and eosin (H&E) (scale bars, 20 μm) and analyzed. Multiple organ injury representations, including interalveolar septum thickened in lung, tubular epithelial cell swelling in kidney, inflammatory cell infiltration in liver and heart, and nuclear debris from dying cells in spleen, are marked with arrows. The corresponding (**B**) lung, (**C**) kidney, (**D**) liver and (**E**) heart injury scores were determined and calculated according to established criteria. Differences were assessed via one-way analysis of variance (ANOVA) with Tukey's multiple comparison tests (n=6 mice per group; $^{*}P<0.05$, $^{**}P<0.01$, $^{***}P<0.001$). The data are expressed as the means ± SEM.

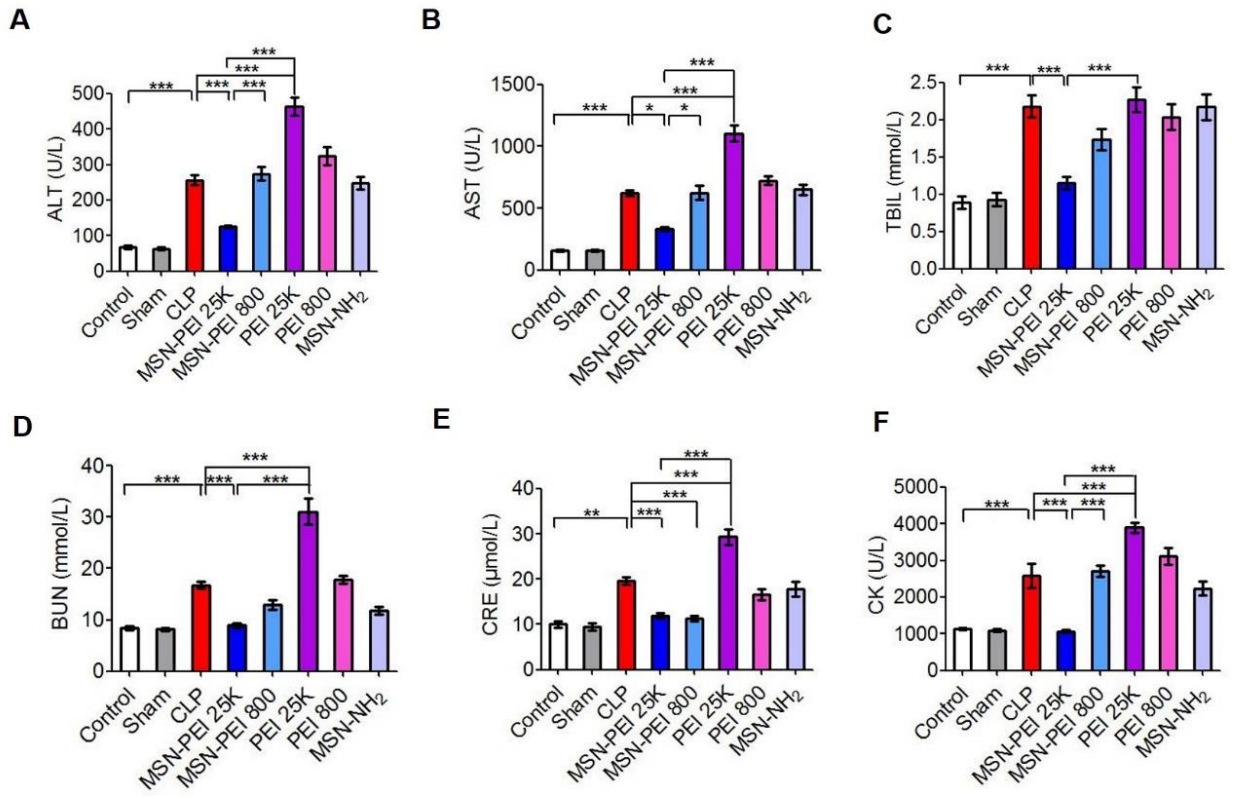

Fig. S13. MSN-PEI 25K attenuates biochemistry parameters in CLP-induced severe sepsis. High-grade CLP was performed on BALB/c mice, followed by treatment as described in **Fig. 4**. The blood serum biochemistry parameters (**A**) ALT, (**B**) AST, (**C**) TBIL, (**D**) BUN, (**E**) CRE, and (**F**) CK were measured. Differences were assessed via one-way analysis of variance (ANOVA) with Tukey's multiple comparison tests (n=6 mice per group; $^{*}P<0.05$, $^{**}P<0.01$, $^{***}P<0.001$). The data are expressed as the means ± SEM.

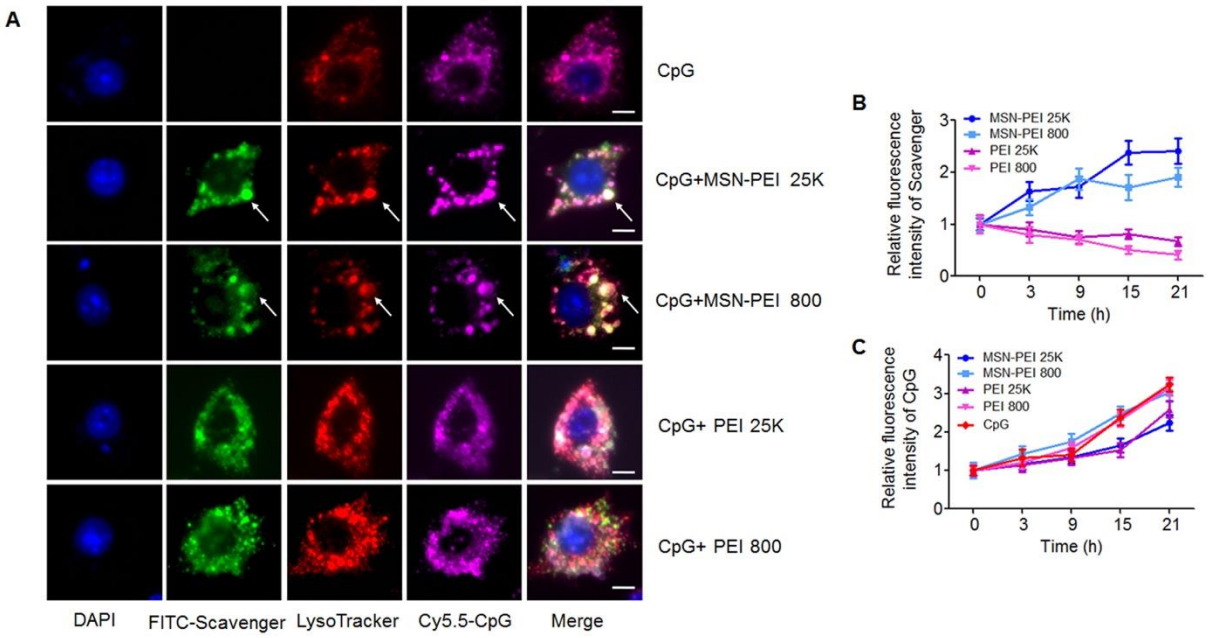

Fig. S14. MSN-PEI 25K exhibits higher cellular retention than PEI-25K. (**A**) Fluorescence images showing intracellular localization of FITC-labeled scavengers and Cy5.5-labeled CpG in RAW 264.7 cells after 6 h of incubation (scale bars, 5 μm). The large white spots in NABN-treated cells are marked with an arrow. (**B** and **C**) RAW 264.7 cells were incubated with Cy5.5-CpG and FITC-NABNs or -NABPs for 3 h, and then, the cell medium was replaced with fresh medium, and cells were incubated for another 3, 6, 12, 18 and 24 h. The relative fluorescence intensity of (**B**) scavengers and (**C**) CpG in cells at each time point was determined via FACS. The data are expressed as the means ± SEM (n=3 independent experiments in triplicate).

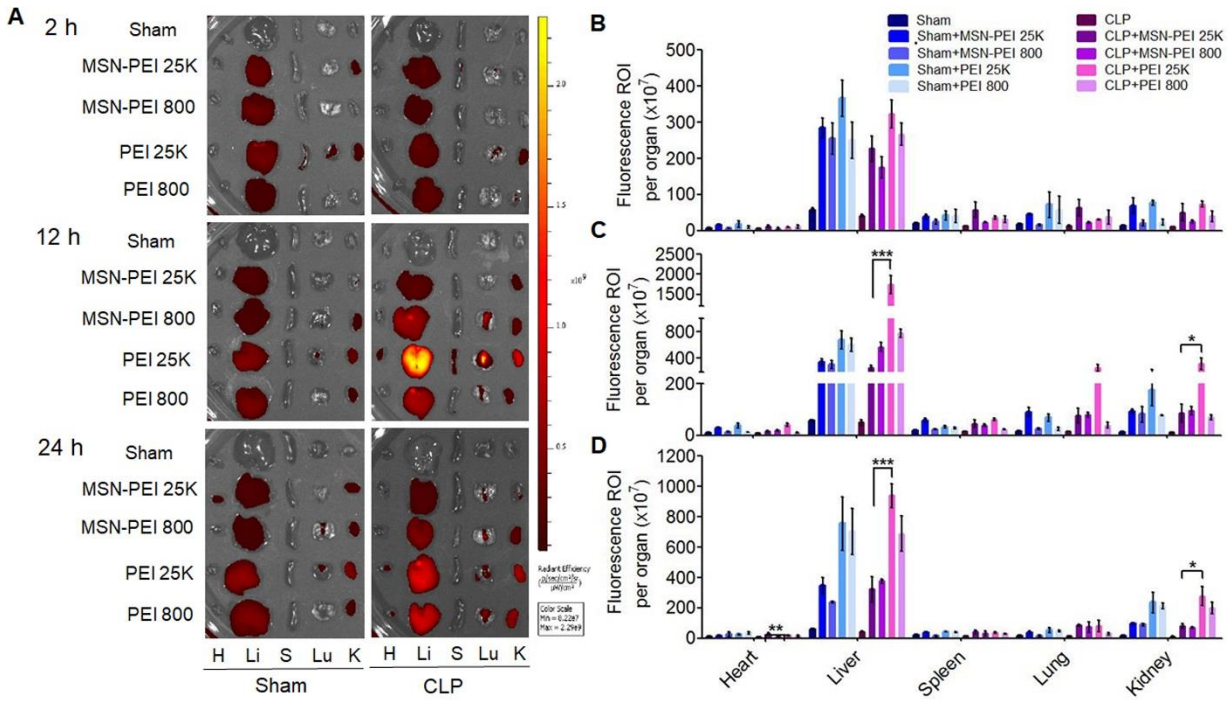

Fig. S15. MSN-PEI 25K shows preferential accumulation and retention in inflamed tissues with negligible toxicity *in vivo*. Near-infrared fluorescence (NIRF) images of (**A**) sham and CLP mice 2, 12 and 24 hr after i.p. injection of Cy7-labeled NABNs or NABPs (20 mg/kg). H (Heart), Lu (Lung), S (Spleen), Li (Liver), K (Kidney). (**B-D**) Semi-quantitative analysis of *ex vivo* fluorescence images of the organs in **A** obtained at (**B**) 2 h, (**C**) 12 h, and (**D**) 24 h. Differences were assessed via one-way analysis of variance (ANOVA) with Tukey's multiple comparison tests (n=3 mice per group; $^{**}P<0.01$, $^{***}P<0.001$). The data are expressed as the means ± SEM.

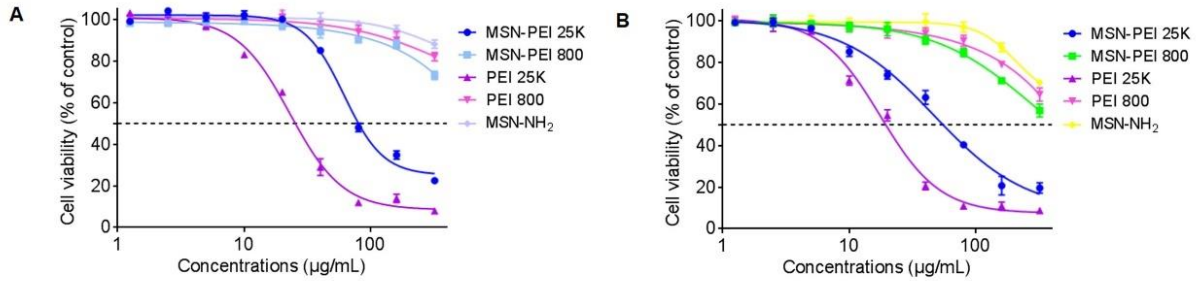

Fig. S16. MSN-PEI 25K has lower cytotoxicity than PEI-25K. Cell viability of (**A**) RAW264.7 cells and (**B**) HUVECs treated with MSN-PEI 25K, MSN-PEI 800, PEI 25K, PEI 800 or MSN-NH_2 at various concentrations for 24 h. The data are expressed as the means ± SEM (n=6 independent experiments in triplicate).

Table S2. Mortality in the repeated-dose toxicity test of NABNs or NABPs. Normal mice were injected (i.p.) three times with different concentrations of MSN-PEI 25K, MSN-PEI 800, PEI 25K, PEI 800 or MSN-NH_2 at 0, 13, and 24 hours. All mice were observed for 14 days after exposure. Mortality was recorded, and all the surviving mice were sacrificed.

	MSN-PEI 25K (n=10)	MSN-PEI 800 (n=10)	PEI 25K (n=10)	PEI 800 (n=10)
Dosages (mg/kg)	Mortality (%)	Mortality (%)	Mortality (%)	Mortality (%)
10	0	0	0	0
20	0	0	20	0
40	0	0	100	100
80	0	0	100	100
160	0	0	100	100
320	0	0	100	100
640	50	20	100	100

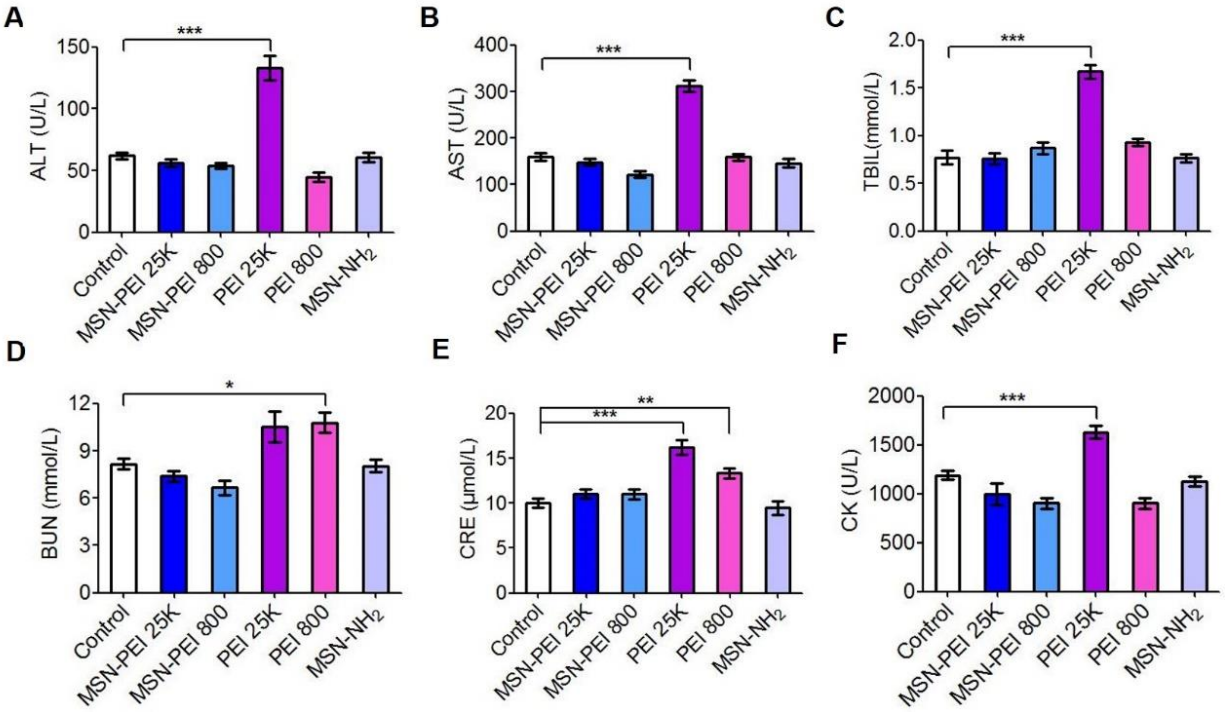

Fig. S17. MSN-PEI 25K shows lower toxicity than PEI-25K *in vivo* as reflected in biochemical profiles. Normal mice were injected (i.p.) three times with 20 mg/kg MSN-PEI 25K, MSN-PEI 800, PEI 25K, PEI 800 or MSN-NH_2 at 0, 13, and 24 hours. (**A**) ALT, (**B**) AST, (**C**) TBIL, (**D**) BUN, (**E**) CRE, and (**F**) CK were measured in serum after 24 h of exposure. Differences were assessed via one-way analysis of variance (ANOVA) with Tukey's multiple comparison tests (n=6 mice per group; $^{*}P<0.05$, $^{**}P<0.01$, $^{***}P<0.001$). The data are expressed as the means ± SEM.

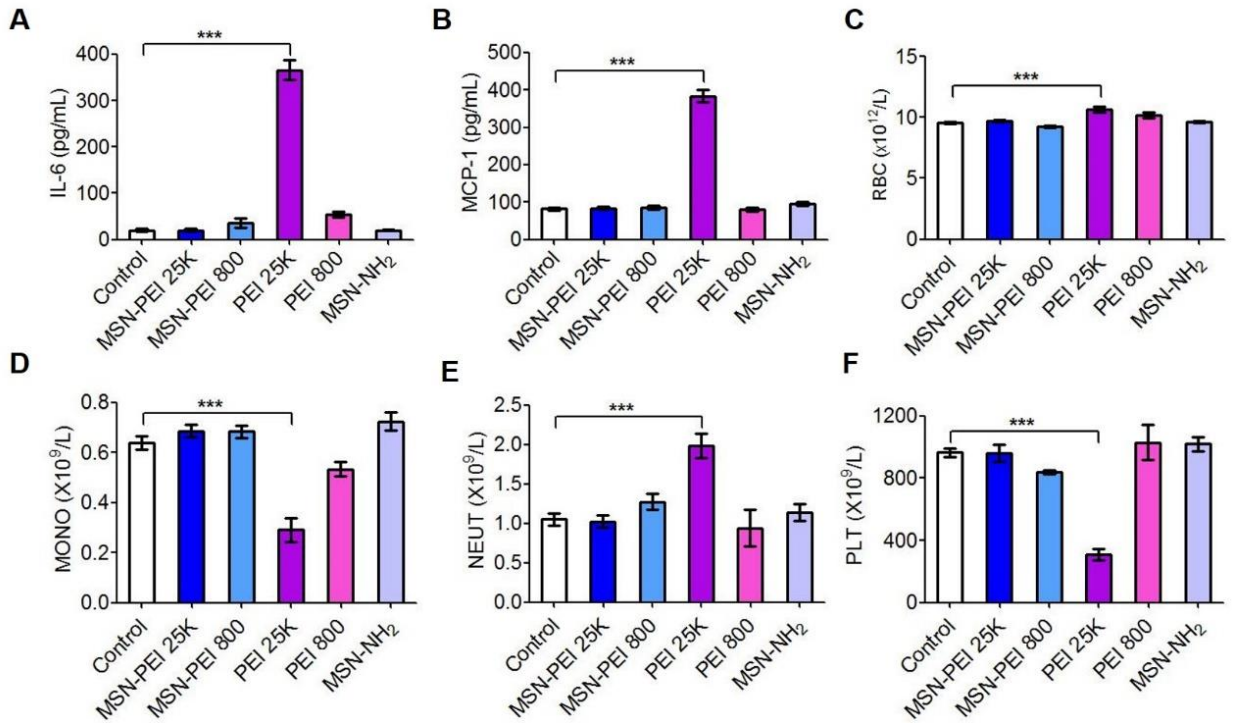

Fig. S18. MSN-PEI 25K shows lower toxicity than PEI-25K *in vivo* as reflected in inflammation responses. Normal mice were injected (i.p.) three times with 20 mg/kg MSN-PEI 25K, MSN-PEI 800, PEI 25K, PEI 800 or MSN-NH_2 at 0, 13, and 24 hours. (**A**) IL-6 levels, (**B**) MCP-1 levels, (**C**) red blood cell (RBC) count, (**D**) monocyte (MONO) count, (**E**) neutrophil (NEUT) count, and (**F**) platelet (PLT) count in the blood were assessed after 24 h of exposure. Differences were assessed via one-way analysis of variance (ANOVA) with Tukey's multiple comparison tests (n=6 mice per group; $^{*}P<0.05$, $^{***}P<0.001$). The data are expressed as the means ± SEM.

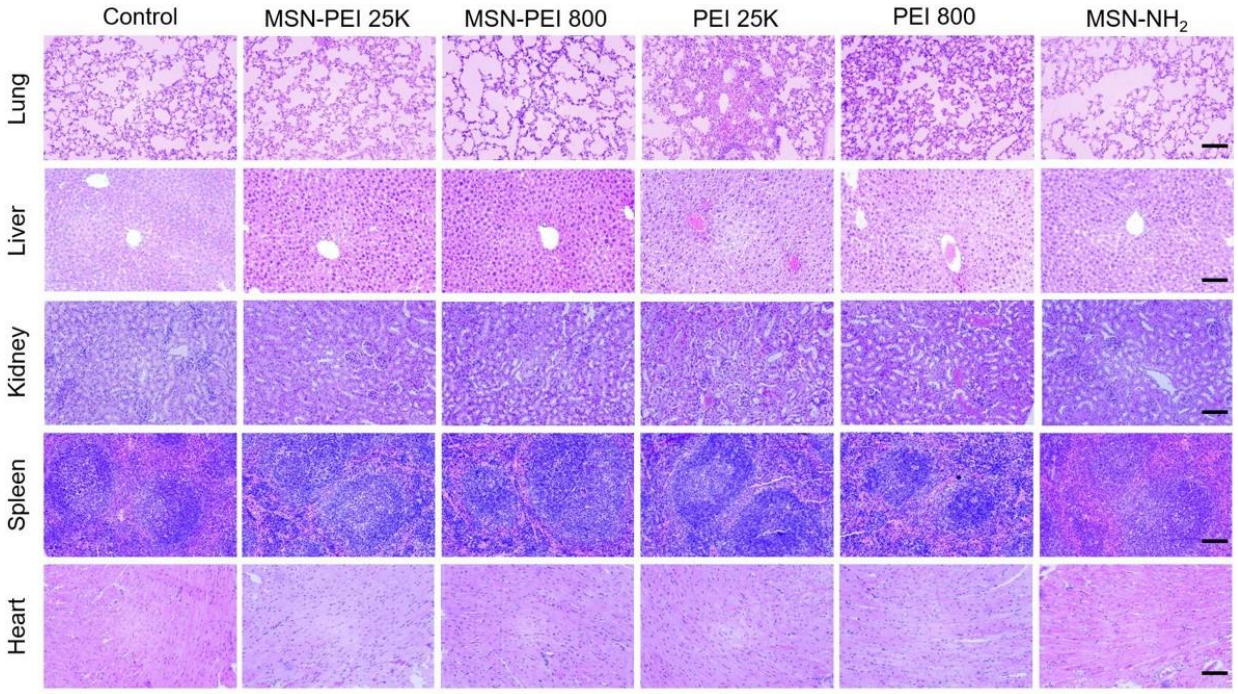

Fig. S19. MSN-PEI 25K shows negligible acute toxicity compared with PEI-25K as reflected in histology. Normal mice were injected (i.p.) three times with 20 mg/kg MSN-PEI 25K, MSN-PEI 800, PEI 25K, PEI 800 or MSN-NH_2 at 0, 13, and 24 hours. Tissue hematoxylin and eosin (H&E) staining (scale bars, 100 μm) of the lung, kidney, heart, liver and spleen was assayed 24 h after the last injection.

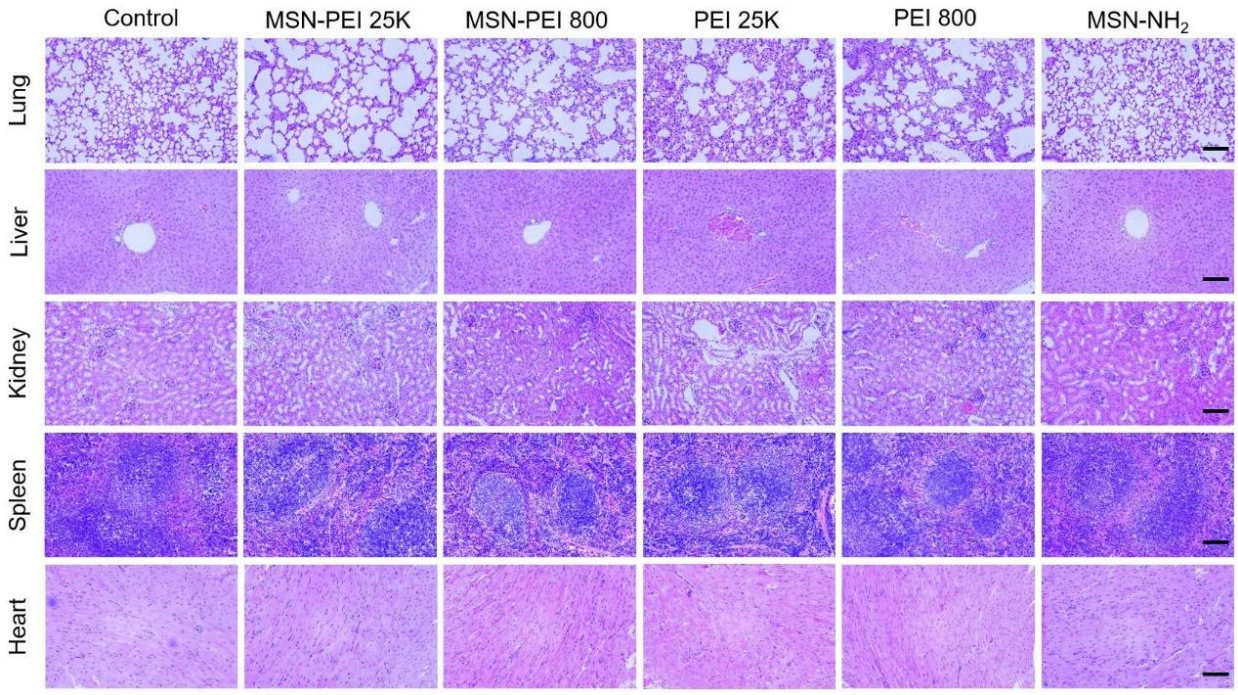

Fig. S20. MSN-PEI 25K shows negligible toxicity compared with PEI-25K seven days after the last administration, as reflected in histology. Normal mice were injected (i.p.) three times with 20 mg/kg MSN-PEI 25K, MSN-PEI 800, PEI 25K, PEI 800 or MSN-NH_2 at 0, 13, and 24 hours. 7 days after the last injection, the lung, kidney, heart, liver and spleen tissues were collected, stained with hematoxylin and eosin (H&E) (scale bars, 100 μm) and evaluated.

REFERENCES AND NOTES

1. C. Rhee, R. Dantes, L. Epstein, D. J. Murphy, C. W. Seymour, T. J. Iwashyna, S. S. Kadri, D. C. Angus, R. L. Danner, A. E. Fiore, J. A. Jernigan, G. S. Martin, E. Septimus, D. K. Warren, A. Karcz, C. Chan, J. T. Menchaca, R. Wang, S. Gruber, M. Klompas; CDC Prevention Epicenter Program, Incidence and trends of sepsis in US hospitals using clinical vs claims data, 2009-2014. *JAMA* **318**, 1241–1249 (2017).

2. R. P. Dellinger, M. M. Levy, A. Rhodes, D. Annane, H. Gerlach, S. M. Opal, J. E. Sevransky, C. L. Sprung, I. S. Douglas, R. Jaeschke, T. M. Osborn, M. E. Nunnally, S. R. Townsend, K. Reinhart, R. M. Kleinpell, D. C. Angus, C. S. Deutschman, F. R. Machado, G. D. Rubenfeld, S. Webb, R. J. Beale, J.-L. Vincent, R. Moreno; The Surviving Sepsis Campaign Guidelines Committee including The Pediatric Subgroup, Surviving Sepsis Campaign: International guidelines for management of severe sepsis and septic shock, 2012. *Intensive Care Med.* **39**, 165–228 (2013).

3. C. Arnold, News feature: The quest to solve sepsis. *Proc. Natl. Acad. Sci. U.S.A.* **115**, 3988–3991 (2018).

4. D. C. Angus, T. van der Poll, Severe sepsis and septic shock. *N. Engl. J .Med.* **369**, 840–851 (2013).

5. R. S. Hotchkiss, I. E. Karl, The pathophysiology and treatment of sepsis. *N. Engl. J .Med.* **348**, 138–150 (2003).

6. K.-M. Kaukonen, M. Bailey, D. Pilcher, D. J. Cooper, R. Bellomo, Systemic inflammatory response syndrome criteria in defining severe sepsis. *N. Engl. J. Med.* **372**, 1629–1638 (2015).

7. M. Bosmann, P. A. Ward, The inflammatory response in sepsis. *Trends Immunol.* **34**, 129–136 (2013).

8. T. van der Poll, F. L. van de Veerdonk, B. P. Scicluna, M. G. Netea, The immunopathology of sepsis and potential therapeutic targets. *Nat. Rev. Immunol.* **17**, 407–420 (2017).

9. K. Saukkonen, P. Lakkisto, V. Pettila, M. Varpula, S. Karlsson, E. Ruokonen, K. Pulkki; Finnsepsis Study Group, Cell-free plasma DNA as a predictor of outcome in severe sepsis and septic shock. *Clin. Chem.* **54**, 1000–1007 (2008).

10. D. J. Dwivedi, L. J. Toltl, L. L. Swystun, J. Pogue, K. L. Liaw, J. I. Weitz, D. J. Cook, A. E. Fox-Robichaud, P. C. Liaw; Canadian Critical Care Translational Biology Group, Prognostic utility and characterization of cell-free DNA in patients with severe sepsis. *Crit. Care* **16**, R151 (2012).

11. H. Kilpinen, S. M. Waszak, A. R. Gschwind, S. K. Raghav, R. M. Witwicki, A. Orioli, E. Migliavacca, M. Wiederkehr, M. Gutierrez-Arcelus, N. I. Panousis, A. Yurovsky, T. Lappalainen, L. Romano-Palumbo, A. Planchon, D. Bielser, J. Bryois, I. Padioleau, G. Udin, S. Thurnheer, D. Hacker, L. J. Core, J. T. Lis, N. Hernandez, A. Reymond, B. Deplancke, E. T. Dermitzakis, Coordinated effects of sequence variation on DNA binding, chromatin structure, and transcription. *Science* **342**, 744–747 (2013).

12. U. Lachelt, E. Wagner, Nucleic acid therapeutics using polyplexes: A journey of 50 years (and beyond). *Chem. Rev.* **115**, 11043–11078 (2015).

13. J. Lee, J. W. Sohn, Y. Zhang, K. W. Leong, D. Pisetsky, B. A. Sullenger, Nucleic acid-binding polymers as anti-inflammatory agents. *Proc. Natl. Acad. Sci. U.S.A.* **108**, 14055–14060 (2011).

14. D. S. Pisetsky, J. Lee, K. W. Leong, B. A. Sullenger, Nucleic acid-binding polymers as anti-inflammatory agents: Reducing the danger of nuclear attack. *Expert Rev. Clin. Immunol.* **8**, 1–3 (2012).

15. N. A. Stearns, J. Lee, K. W. Leong, B. A. Sullenger, D. S. Pisetsky, The inhibition of anti-DNA binding to DNA by nucleic acid binding polymers. *PLOS ONE* **7**, e40862 (2012).

16. I. Naqvi, R. Gunaratne, J. E. McDade, A. Moreno, R. E. Rempel, D. C. Rouse, S. G. Herrera, D. S. Pisetsky, J. Lee, R. R. White, B. A. Sullenger, Polymer-mediated inhibition of pro-invasive nucleic acid DAMPs and microvesicles limits pancreatic cancer metastasis. *Mol. Ther.* **26**, 1020–1031 (2018).

17. E. K. Holl, K. L. Shumansky, L. B. Borst, A. D. Burnette, C. J. Sample, E. A. Ramsburg, B. A. Sullenger, Scavenging nucleic acid debris to combat autoimmunity and infectious disease. *Proc. Natl. Acad. Sci. U.S.A.* **113**, 9728–9733 (2016).

18. J. C. Roberts, M. K. Bhalgat, R. T. Zera, Preliminary biological evaluation of polyamidoamine (PAMAM) Starburst^{TM} dendrimers. *J. Biomed. Mater. Res.* **30**, 53–65 (1996).

19. C. F. Jones, R. A. Campbell, A. E. Brooks, S. Assemi, S. Tadjiki, G. Thiagarajan, C. Mulcock, A. S. Weyrich, B. D. Brooks, H. Ghandehari, D. W. Grainger, Cationic PAMAM dendrimers aggressively initiate blood clot formation. *ACS Nano* **6**, 9900–9910 (2012).

20. C. F. Jones, R. A. Campbell, Z. Franks, C. C. Gibson, G. Thiagarajan, A. Vieira-de-Abreu, S. Sukavaneshvar, S. F. Mohammad, D. Y. Li, H. Ghandehari, A. S. Weyrich, B. D. Brooks, D. W. Grainger, Cationic PAMAM dendrimers disrupt key platelet functions. *Mol. Pharm.* **9**, 1599–1611 (2012).

21. H. Liang, B. Peng, C. Dong, L. Liu, J. Mao, S. Wei, X. Wang, H. Xu, J. Shen, H.-Q. Mao, X. Gao, K. W. Leong, Y. Chen, Cationic nanoparticle as an inhibitor of cell-free DNA-induced inflammation. *Nat. Commun.* **9**, 4291 (2018).

22. J. A. Buras, B. Holzmann, M. Sitkovsky, Animal models of sepsis: Setting the stage. *Nat. Rev. Drug Discov.* **4**, 854–865 (2005).

23. D. Rittirsch, M. S. Huber-Lang, M. A. Flierl, P. A. Ward, Immunodesign of experimental sepsis by cecal ligation and puncture. *Nat. Protoc.* **4**, 31–36 (2009).

24. H. Shi, Y. Hong, J. Qian, X. Cai, S. Chen, Xuebijing in the treatment of patients with sepsis. *Am. J. Emerg. Med.* **35**, 285–291 (2017).

25. Q. Wang, X. Wu, X. Tong, Z. Zhang, B. Xu, W. Zhou, Xuebijing ameliorates sepsis-induced lung injury by downregulating HMGB1 and RAGE expressions in mice. *Evid.-Based Complementary Altern. Med.* **2015**, 860259 (2015).

26. X. Meng, W. Sun, Y. Ren, Y. Xiao, P. Zhao, W. Lu, L. Hua, L. Wang, L. Wang, Y. Yu, Protective role of surface Toll-like receptor 9 expressing neutrophils in local inflammation during systemic inflammatory response syndrome in mice. *Mol. Immunol.* **90**, 74–86 (2017).

27. N. Z. Knežević, J.-O. Durand, Large pore mesoporous silica nanomaterials for application in delivery of biomolecules. *Nanoscale* **7**, 2199–2209 (2015).

28. D. Shao, M. Li, Z. Wang, X. Zheng, Y.-H. Lao, Z. Chang, F. Zhang, M. Lu, J. Yue, H. Hu, H. Yan, L. Chen, W.-f. Dong, K. W. Leong, Bioinspired diselenide-bridged mesoporous silica nanoparticles for dual-responsive protein delivery. *Adv. Mater.* **30**, 1801198 (2018).

29. C. Pinese, J. Lin, U. Milbreta, M. Li, Y. Wang, K. W. Leong, S. Y. Chew, Sustained delivery of siRNA/mesoporous silica nanoparticle complexes from nanofiber scaffolds for long-term gene silencing. *Acta Biomater.* **76**, 164–177 (2018).

30. T. J. Graetz, R. S. Hotchkiss, Sepsis: Preventing organ failure in sepsis—The search continues. *Nat. Rev. Nephrol.* **13**, 5–6 (2017).

31. A. Nel, T. Xia, H. Meng, X. Wang, S. Lin, Z. Ji, H. Zhang, Nanomaterial toxicity testing in the 21st century: Use of a predictive toxicological approach and high-throughput screening. *Acc. Chem. Res.* **46**, 607–621 (2013).

32. J. Stoller, L. Halpin, M. Weis, B. Aplin, W. Qu, C. Georgescu, M. Nazzal, Epidemiology of severe sepsis: 2008-2012. *J. Crit. Care* **31**, 58–62 (2016).

33. Q. Zhang, M. Raoof, Y. Chen, Y. Sumi, T. Sursal, W. Junger, K. Brohi, K. Itagaki, C. J. Hauser, Circulating mitochondrial DAMPs cause inflammatory responses to injury. *Nature* **464**, 104–107 (2010).

34. J.-W. Kang, S.-J. Kim, H.-I. Cho, S.-M. Lee, DAMPs activating innate immune responses in sepsis. *Ageing Res. Rev.* **24**, 54–65 (2015).

35. B. McDonald, R. Urrutia, B. G. Yipp, C. N. Jenne, P. Kubes, Intravascular neutrophil extracellular traps capture bacteria from the bloodstream during sepsis. *Cell Host Microbe* **12**, 324–333 (2012).

36. A. Yadav, V. Saini, S. Arora, MCP-1: Chemoattractant with a role beyond immunity: A review. *Clin. Chim. Acta* **411**, 1570–1579 (2010).

37. T. Xia, M. Kovochich, M. Liong, H. Meng, S. Kabehie, S. George, J. I. Zink, A. E. Nel, Polyethyleneimine coating enhances the cellular uptake of mesoporous silica nanoparticles and allows safe delivery of siRNA and DNA constructs. *ACS Nano* **3**, 3273–3286 (2009).

38. J. G. Croissant, Y. Fatieiev, N. M. Khashab, Degradability and clearance of silicon, organosilica, silsesquioxane, silica mixed oxide, and mesoporous silica nanoparticles. *Adv. Mater.* **29**, 1604634 (2017).

39. X. Du, F. Kleitz, X. Li, H. Huang, X. Zhang, S.-Z. Qiao, Disulfide-bridged organosilica frameworks: Designed, synthesis, redox-triggered biodegradation, and nanobiomedical applications. *Adv. Funct. Mater.* **28**, 1707325 (2018).

40. K. Timmermans, M. Kox, G. J. Scheffer, P. Pickkers, Plasma nuclear and mitochondrial DNA levels, and markers of inflammation, shock, and organ damage in patients with septic shock. *Shock* **45**, 607–612 (2016).

41. E. Mastrobattista, W. E. Hennink, Polymers for gene delivery: Charged for success. *Nat. Mater.* **11**, 10–12 (2011).

42. Y. Ren, X. Jiang, D. Pan, H.-Q. Mao, Charge density and molecular weight of polyphosphoramidate gene carrier are key parameters influencing its DNA compaction ability and transfection efficiency. *Biomacromolecules* **11**, 3432–3439 (2010).

43. C. L. Grigsby, K. W. Leong, Balancing protection and release of DNA: Tools to address a bottleneck of non-viral gene delivery. *J. R. Soc. Interface* **7**, (suppl 1), S67–S82 (2010).

44. D. Fischer, T. Bieber, Y. Li, H.-P. Elsässer, T. Kissel, A novel non-viral vector for DNA delivery based on low molecular weight, branched polyethylenimine: Effect of molecular weight on transfection efficiency and cytotoxicity. *Pharm. Res.* **16**, 1273–1279 (1999).

45. B. J. Crielaard, T. Lammers, R. M. Schiffelers, G. Storm, Drug targeting systems for inflammatory disease: One for all, all for one. *J. Control. Release* **161**, 225–234 (2012).

46. H. Nehoff, N. N. Parayath, L. Domanovitch, S. Taurin, K. Greish, Nanomedicine for drug targeting: Strategies beyond the enhanced permeability and retention effect. *Int. J. Nanomedicine* **9**, 2539–2555 (2014).

47. S. J. Soenen, P. Rivera-Gil, J.-M. Montenegro, W. J. Parak, S. C. De Smedt, K. Braeckmans, Cellular toxicity of inorganic nanoparticles: Common aspects and guidelines for improved nanotoxicity evaluation. *Nano Today* **6**, 446–465 (2011).

48. M. Soh, D.-W. Kang, H.-G. Jeong, D. Kim, D. Y. Kim, W. Yang, C. Song, S. Baik, I.-Y. Choi, S. K. Ki, H. J. Kwon, T. Kim, C. K. Kim, S.-H. Lee, T. Hyeon, Ceria-Zirconia nanoparticles as an enhanced multi-antioxidant for sepsis treatment. *Angew. Chem. Int. Ed.* **56**, 11399–11403 (2017).

49. S. Spence, M. K. Greene, F. Fay, E. Hams, S. P. Saunders, U. Hamid, M. Fitzgerald, J. Beck, B. K. Bains, P. Smyth, E. Themistou, D. M. Small, D. Schmid, C. M. O'Kane, D. C. Fitzgerald, S. M. Abdelghany, J. A. Johnston, P. G. Fallon, J. F. Burrows, D. F. McAuley, A. Kissenpfennig, C. J. Scott, Targeting Siglecs with a sialic acid-decorated nanoparticle abrogates inflammation. *Sci. Transl. Med.* **7**, 303ra140 (2015).

50. C. W. Seymour, V. X. Liu, T. J. Iwashyna, F. M. Brunkhorst, T. D. Rea, A. Scherag, G. Rubenfeld, J. M. Kahn, M. Shankar-Hari, M. Singer, C. S. Deutschman, G. J. Escobar, D. C. Angus, Assessment of clinical criteria for sepsis: For the third international consensus definitions for sepsis and septic shock (sepsis-3). *JAMA* **315**, 762–774 (2016).

51. X. Huang, F. Venet, Y. L. Wang, A. Lepape, Z. Yuan, Y. Chen, R. Swan, H. Kherouf, G. Monneret, C. S. Chung, A. Ayala, PD-1 expression by macrophages plays a pathologic role in altering microbial clearance and the innate inflammatory response to sepsis. *Proc. Natl. Acad. Sci. U.S.A.* **106**, 6303–6308 (2009).

52. H. Li, S. Wang, B. Zhan, W. He, L. Chu, D. Qiu, N. Li, Y. Wan, H. Zhang, X. Chen, Q. Fang, J. Shen, X. Yang, Therapeutic effect of Schistosoma japonicum cystatin on bacterial sepsis in mice. *Parasit. Vectors* **10**, 222 (2017).

53. S. Stewart, G. L. Winters, M. C. Fishbein, H. D. Tazelaar, J. Kobashigawa, J. Abrams, C. B. Andersen, A. Angelini, G. J. Berry, M. M. Burke, A. J. Demetris, E. Hammond, S. Itescu, C. C. Marboe, B. McManus, E. F. Reed, N. L. Reinsmoen, E. R. Rodriguez, A. G. Rose, M. Rose, N. Suciu-Focia, A. Zeevi, M. E. Billingham, Revision of the 1990 working formulation for the standardization of nomenclature in the diagnosis of heart rejection. *J. Heart Lung Transplant.* **24**, 1710–1720 (2005).